Journal of Coastal Research	17	3	658–671	West Palm Beach, Florida	Summer 2001

Estimating Wave Elevation from Pressure Using Second Order Nonlinear Wave-Wave Interaction Theory with Applications to Hurricane Andrew

Steven F. DiMarco*, E. Meza†,[1], and J. Zhang†

*Department of Oceanography
Texas A & M University
College Station, TX 77843,
U.S.A.

†Ocean Engineering Program
Department of Civil
Engineering
Texas A & M University
College Station, TX 77843,
U.S.A.

ABSTRACT

DIMARCO, S.F.; MEZA, E., and ZHANG, J., 2001. Estimating wave elevation from pressure using second order nonlinear wave-wave interaction theory with applications to Hurricane Andrew. *Journal of Coastal Research,* 17(3), 658–671. West Palm Beach (Florida), ISSN 0749-0208.

We present a methodology to determine the nonlinear relationship between an observed dynamic pressure time series at a fixed point below the surface and the surface elevation. This method extends the formalism of previous studies where the analytical relationship between surface elevation and potential in both unidirectional and directional irregular wave trains has been derived up to second order in wave steepness. Laboratory wave tank tests show that the predicted wave elevation from the nonlinear model is more accurate than the predicted linear surface elevation of a transient irregular wave train, especially for deep troughs and high wave crests.

We apply the nonlinear theory of estimate wave elevation of a unique pressure time series recorded at a site 20 km south of Terrebonne Bay, Louisiana, during Hurricane Andrew and compare that result to the wave elevation estimated from the same time series using linear wave theory. The site was within 30 km of the storm's eye at closest approach. The maximum significant wave height using nonlinear wave theory is reduced by 8.4% to 7.69 m. The nonlinear interaction is seen to be strongest during the six-hour period that hurricane force winds were present at the site.

ADDITIONAL INDEX WORDS: *Gulf of Mexico, time-series analysis, wave observations, wave tank, pressure gauges.*

INTRODUCTION

We apply a nonlinear hybrid methodology to a bottom pressure time series. The nonlinear methodology was used originally to provide accurate predictions of irregular wave kinematics and short-distance wave evolution based on a surface elevation time series measured at a fixed point (ZHANG *et al.,* 1993; ZHANG *et al.,* 1996; SPELL *et al.,* 1996; ZHANG *et al.,* 1999a; ZHANG *et al.,* 1999b). In these previous studies, the analytical relationship between surface elevation and potential in both unidirectional and directional irregular wave train has been derived up to second order in wave steepness. For this study, we extend the formalism to determine the nonlinear relation between an observed dynamic pressure at a fixed point below the surface and the surface elevation. Strong evidence of this relationship has also been investigated by HERBERS and GUZA (1991, 1994) for pressure measurements at the ocean bottom. They used second-order statistics (HERBERS and GUZA, 1991 and 1994) and bispectral analysis (HERBERS and GUZA, 1992) to confirm their observations. This formalism does not consider far-field, weak, third-order nonlinear interactions (PHILLIPS, 1960; HASSELMANN, 1962; YUEN and LAKE, 1982).

Because linear and nonlinear surface components are attenuated differently at depth, a surface wave spectrum estimated from a near-bottom recorded pressure time series containing nonlinear energy components will be overestimated when using linear theory alone to adjust for the effects of hydrodynamic attenuation. The magnitude of overestimation is related to the amount of nonlinear interaction in the original pressure time series. The pressure measurements, which include all orders of interaction, must be separated into linear (first-order) and nonlinear (second-order) components to prevent the second-order components from being treated as first-order components and thereby artificially increase the estimated wave height. An accurate estimation of a wave field during extreme events is of immense importance to the offshore drilling industry and is considered crucial for the survival conditions of offshore structure design.

In Section 2, we present the mathematical formalism of the nonlinear wave theory. The formalism is then tested in Section 3 by comparing the measured wave elevation (using wave staffs) of an experimentally generated irregular wave train with the predicted linear and nonlinear wave eleva-

98231 received 30 September 1998; accepted in revision 17 September 2000.

[1] Present address: Centro de Investigacion en Ciencia Aplicada y Tecnologia, Avanzada del Instituto Politechnico Nacional (CICATA-IPN), Altamira, Tamaulipas, Mexico, C.P. 89600.

tions. Section 4 provides a brief description of observational data measured during a hurricane. Finally in Section 5, the nonlinear model is applied to hurricane data to obtain a more accurate estimate for the significant wave height and wave spectrum.

METHODOLOGY

An irregular wave train composed of many free-wave (linear) components may generate bound-wave components by interacting with each other. The newly generated bound-wave components do not satisfy the usual linear dispersion relation. When analyzing wave dynamics using linear theory alone, therefore, the contribution of bound-wave components is wrongly treated as free-wave energy. In certain cases, the description of wave kinematics near steep wave crests and dynamic pressure under a deep trough using linear wave theory is known to be inaccurate (RODENBUSCH and FORRISTALL, 1986; ZHANG *et al.*, 1991). Therefore, to accurately predict wave characteristics based on measured wave elevation, the contributions from free-wave and bound-wave components should be computed separately using the different relationships between their elevation and potential. To do this, the wave field is decomposed into free- and bound-wave components. The nonlinear decomposition is performed by subtracting the contribution of bound-wave components from the measured wave elevation and then decomposing the irregular wave train into free-wave components.

Because the computation of the bound-wave components requires information about the free-wave components, the decomposition is iterative. The amplitude and phase spectra of the dynamic pressure observations are initially considered to be a free-wave spectra. Interaction spectra are then estimated from the initial spectra. The spectral interaction components are then subtracted from the free-wave components. This process is iterated until the interaction terms converge to preset tolerances. It has been shown that the prediction of wave kinematics and surface elevation using nonlinear wave theory provides better agreement with direct measurements than do the predictions using linear wave theory (SPELL *et al.*, 1996).

Using the formulation of the wave elevation and potential derived in the nonlinear hybrid wave model (ZHANG *et al.*, 1996), the nonlinear dynamic pressure solution is obtained by substituting the nonlinear potential into the Bernoulli Equation. In the nonlinear wave model, the conventional perturbation and phase modulation methods are used to describe the interactions between wave components with close and disparate frequencies, respectively (ZHANG *et al.*, 1993). In this study, the pressure transducer was deployed below the free surface. Because dynamic pressure exponentially decays with distance from the surface, the signal-to-noise ratio of measurements at high frequencies is small; therefore, a relatively low cut-off frequency (0.200 Hz) is set for the surface elevation analysis in Section 5. Because the frequencies of the interacting wave components are relatively close, we use only the conventional perturbation method for the description of the nonlinear interaction among wave components (PRISLIN *et al.*, 1997).

Solutions for the potential function and surface elevation up to second order for two interactive waves in intermediate water depth, using a conventional perturbation approach, were first presented by LONGUET-HIGGINS and STEWART (1960). These solutions assumed incompressible and irrotational flow and constant pressure at the free surface and are known to converge rapidly when modeling the interaction of waves of comparable wave lengths.

The potential function, ϕ and surface elevation, η are expressed as a linear combination of the first- (linear) and second-order (nonlinear) motions of a series of progressive waves as:

$$\phi = \phi^{(1)} + \phi^{(2)} \tag{1}$$

and

$$\eta = \eta^{(1)} + \eta^{(2)}. \tag{2}$$

The total potential in the spectral range of interest is obtained using the conventional perturbation method. The solutions for the first- and second-order potential are:

$$\begin{aligned}\phi = \sum_{j=N_l}^{N_h} \Bigg\{ & \frac{a_j g \cosh(k_j(z+h))}{\sigma_j \cosh(k_j h)} \sin(\theta_j) \\ & + \frac{3 a_j^2 \sigma_j \cosh(2k_j(z+h))}{8 \sinh^4(k_j h)} \sin(2\theta_j) \Bigg\} \\ + \sum_{j=N_l+1}^{N_h} \sum_{i=N_l}^{j-1} \Bigg\{ & -A_{j+i} \frac{\cosh((k_j+k_i)(z+h))}{\cosh((k_j+k_i)h)} \sin(\theta_j+\theta_i) \\ & + A_{j-i} \frac{\cosh((k_j-k_i)(z+h))}{\cosh((k_j-k_i)h)} \sin(\theta_j-\theta_i) \Bigg\},\end{aligned} \tag{3}$$

where N_l and N_h represent low and high frequency limits of the interacting components, respectively. In Eq. 3, the first term is the linear contribution to the potential; the second term corresponds to the second-order second-harmonic terms; and the last summation (a double summation) provides the contribution of the sum- and difference-frequency terms. The sum- and difference-frequency amplitudes, A_+ and A_- in Eq. 3 are given in the Appendix. The nonlinear dynamic pressure is obtained by solving Bernoulli's Equation within the fluid

$$\frac{P}{\rho} + gz + \frac{1}{2}(\nabla\phi)^2 + \frac{\partial\phi}{\partial t} = 0. \tag{4}$$

The pressure solution can also be written as a combination of the linear and nonlinear contributions as above. Substituting the nonlinear potential of Eq. 3 into Eq. 4 yields the total dynamic pressure:

$$\frac{P}{\rho g} + z = \sum_{j=N_l}^{N_h} \left\{ a_j \frac{\cosh(k_j(z+h))}{\cosh(k_j h)} \cos(\theta_j) + a_j{}^2 k_j \frac{1 - \cosh(2k_j(z+h))}{2\sinh(2k_j h)} + a_j{}^2 k_j \frac{3\cosh(2k_j(2k_j(z+h)) - \sinh^2(k_j h)}{2\sinh(2k_j h)\sinh^2(k_j h)} \cos(2\theta_j) \right\} + \sum_{j=N_l+1}^{N_h} \sum_{i=N_l}^{j-1} \left\{ -\left(\frac{k_j(1+\lambda_{i,j})}{\alpha_j \sigma_j} A_{j+i} K_{i,j}{}^{C+} + \frac{a_i a_j k_j \lambda_{i,j}}{2\alpha_j} K_{i,j}{}^{S-} \right) \times \cos(\theta_j + \theta_i) + \left(\frac{k_j(1-\lambda_{i,j})}{2\alpha_j \sigma_j} A_{j-i} K_{i,j}{}^{C-} - \frac{a_i a_j k_j \lambda_{i,j}}{2\alpha_j} K_{i,j}{}^{S+} \right) \times \cos(\theta_j - \theta_i) \right\}. \quad (5)$$

Similar to the potential, the first term in the single summation term is the linear contribution to the total pressure. The second and third terms in the single summation are of second order in wave steepness and represent the second-harmonic hydrostatic (time-independent) and dynamic pressures, respectively. The last term is the contribution from the sum- and difference-frequency interactions.

Similarly, the total wave elevation is

$$\eta = \sum_{j=N_l}^{N_h} \left\{ a_j \cos(\theta_j) + \frac{a_j{}^2 k_j \alpha_j}{4} (3\alpha_j{}^2 - 1)\cos(2\theta_j) \right\} + \sum_{j=N_l+1}^{N_h} \sum_{i=N_l}^{j-1} \times \left\{ -\left(\frac{k_j(1+\lambda_{i,j})}{\alpha_j \sigma_j} A_{j+i} - \frac{a_i a_j k_j}{2\alpha_j} (\lambda_{i,j}{}^2 + \lambda_{i,j}(1 - \alpha_i \alpha_j) + 1) \right) \times \cos(\theta_j + \theta_i) + \left(\frac{k_j(1-\lambda_{i,j})}{\alpha_j \sigma_j} A_{j-i} + \frac{a_i a_j k_j}{2\alpha_j} (\lambda_{i,j}{}^2 - \lambda_{i,j}(1 + \alpha_i \alpha_j) + 1) \right) \times \cos(\theta_j - \theta_i) \right\}. \quad (6)$$

Finally, the nonlinear dispersion relation for each wave component in the wave field is

$$\sigma_i{}^2 = g k_i \tanh(k_i h) \left\{ 1 + a_i{}^2 S_i + \sum_{j=N_l}^{i-1} a_j{}^2 Q_{ij} + \sum_{j=i+1}^{N_h} a_j{}^2 Q_{ji} \right\}. \quad (7)$$

Other parameters in the nonlinear potential, elevation, and dynamic pressure of Eqs. 1–7 are: a_i, k_i, σ_i, and $\theta_i = k_i x - \sigma_i t + \beta_i$ ($i = 1$ or 2) and are the wave amplitude, wave number, angular frequency and the linear phase function with initial phase β of two waves traveling at finite depth h, respectively. The Appendix describes further the second-order contributions, S_i and Q_{ij}, to the nonlinear dispersion relation of Eq. 7. Due to the nonlinear dispersion relation, wavenumbers in a unidirectional irregular wave train are slightly smaller than those described by the corresponding linear dispersion relation.

Figure 1 provides an illustration of the different dynamics associated with free and bound waves and shows the amplitude ratio between the surface elevation and the related dynamic pressure head (in meters) as a function of frequency at a depth of 19.5 m. For comparison to the observational parameters presented in Section 5, the depth parameters during Hurricane Andrew are $h = 20.5$ m and $z = -19.5$ m. The curve corresponding to the free-wave components is constructed from the ratio of the amplitudes of the first terms of Eqs. 5 and 6 and describes the hydrodynamic attenuation of free-wave (linear) components with depth. For the bound-wave components, the curve is constructed from the ratios of second-order terms corresponding to the sum- and difference-frequency components and the second harmonic terms. For this figure, we have taken $\lambda_{i,j} = \omega_1/\omega_2 = 0.8$. It should be noted that the ratios for the second harmonics and sum-frequency bound-wave components of $\lambda_{i,j} = 0.70$ to 0.95 are similar to the ratio found for $\lambda_{i,j} = 0.80$. We see that for frequencies greater than 0.10 Hz, the second-order components are attenuated less than the free-wave components and, therefore, have a smaller ratio. For a given frequency, therefore, the wavenumbers of bound-wave components are smaller than those of free-wave components and, therefore, the exponential decay for the corresponding pressure is smaller. For frequencies less than 0.10 Hz, the attenuation of bound and free waves are essentially the same.

APPLICATION TO LABORATORY WAVE MEASUREMENTS

To validate the nonlinear wave methodology of Section 2 and the corresponding numerical scheme, a steep transient wave train was generated in a two-dimensional wave flume. This section describes the experiment and presents the results of applying the above model to a dynamic pressure time series recorded at an intermediate depth as the transient wave propagated past the pressure sensor. Similar to Hurricane Andrew, the waves generated in this experiment were steep, and pressure measurements were taken relatively far below the free surface (see Section 5).

The experiment was performed at the two-dimensional glass-walled wave flume at the Hydrodynamics Laboratory of Texas A&M University. The flume is 36.1 m in overall length, 0.91 m in width, and 1.22 m in depth. The mean water depth during the experiment was 0.90 m. A downstream absorbing beach, located 31.5 m from the wavemaker, is constructed of fibrous mats 5 cm thick, supported by a perforated metallic sheet on a 1:3.3 slope. Wave generation is provided by a dry-back, hinge-flap wavemaker powered by a brushless synchronous AC-servo motor. Two SENSOTEC Model GW-100 pressure transducers and three resistant-type surface-piercing wave gauges were used to measure pressure and elevation of the transient wave train.

The steep transient wave train was formed by sequentially generating a series of waves from high to low frequencies and superposing at a downstream location. The wave train became very steep and eventually broke. The experiment was

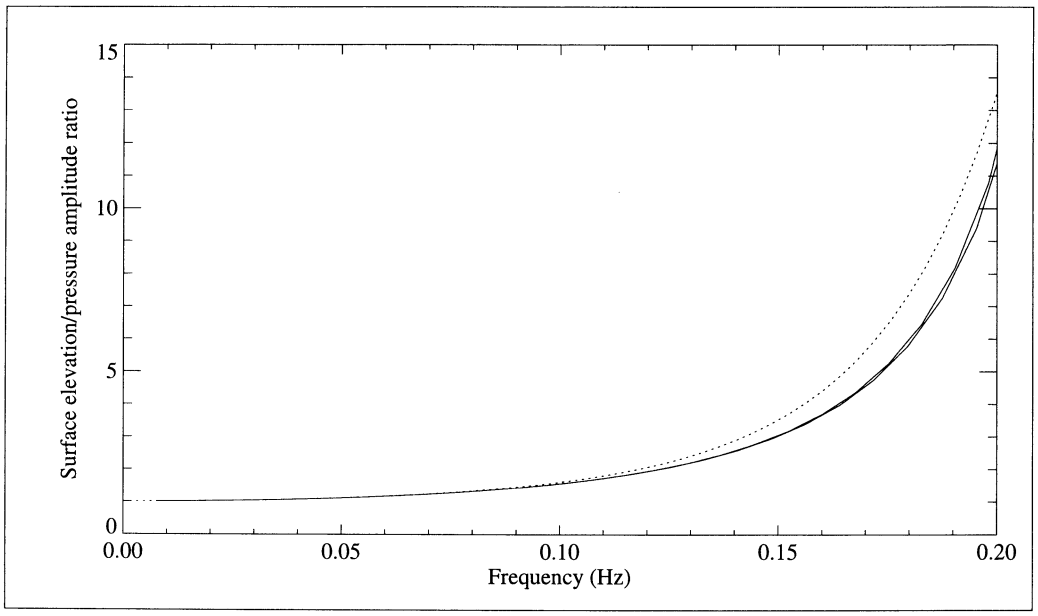

Figure 1. Transfer function of surface elevation to dynamic pressure ratio at a depth of 19.5 m below the surface for free-wave components (dashed) and bound-wave components (solid). Pressure sensor is 1.0 m off bottom and $\lambda_{i,j} = 0.8$.

designed for studying wave energy loss due to wave breaking (ZHANG *et al.,* 1997). For validating the nonlinear wave model, only the measurements before the wave breaking (two elevation records and two pressure records) were used. The positions of the two pressure transducers and two wave gauges in the wave flume are sketched in Figure 2. Plunging type wave-breaking occurred approximately 2.5 m downstream of gauge 1.

Pressure and wave elevation were sampled at a rate of 50 Hz. The pressure transducer was located about 35 cm below the mean water level. The pressure signals were used as the input for decomposing the transient wave train into a series of free-wave components. In the decomposition, the free-wave components were truncated at 1.75 Hz to avoid spurious high-frequency noise contaminating the signal. Pressure as a function of time at the transducer was recovered using the nonlinear wave model and based on the information of decomposed free-wave components. We confirmed that the energy associated with frequencies above 1.75 Hz contributes little to the total variance of the measured time series.

Based on the pressure measurements, the free-wave components of the pressure spectrum were derived using the nonlinear wave theory and then used to predict the resultant elevations of the free- and bound-wave components at gauges 1 and 2, which were located at the surface above the pressure transducers. The predicted and corresponding measured

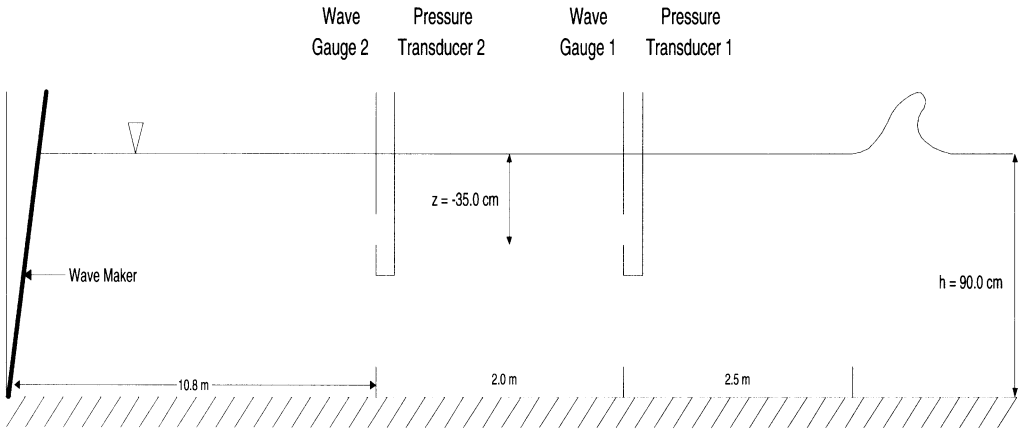

Figure 2. Schematic diagram of wave flume showing locations of wave maker, wave gauges, and pressure transducers (1 and 2).

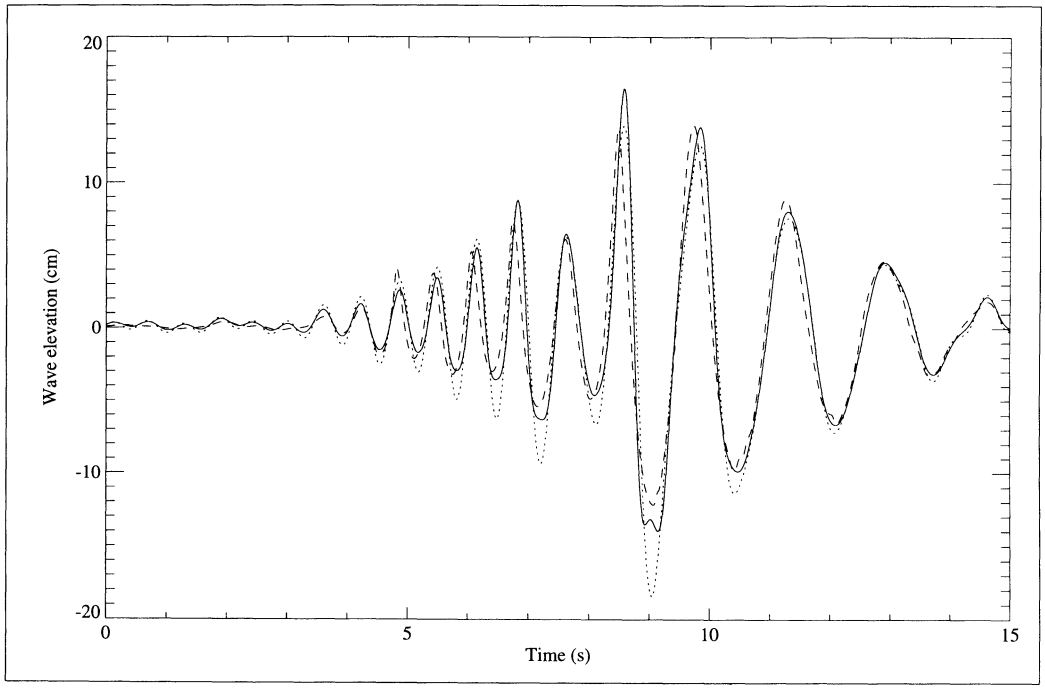

Figure 3. Observed (dashed) and predicted wave elevation at gauge 1 using linear (dotted) and nonlinear (solid) theory.

wave elevations at gauges 1 and 2 are shown in Figures 3 and 4. For comparison, the predicted wave elevations for both the nonlinear and linear wave theories are plotted in these two figures. Overall, Figures 3 and 4 show that the predictions obtained using nonlinear theory are very close to the corresponding measurements, and the discrepancies between them at the steep wave crests and troughs are small. However, the discrepancies between the predictions of linear wave theory and the measurements are relatively large. At the crests and troughs of waves of large wave heights, linear wave theory greatly underpredicts and overpredicts the wave elevation. The greatest over-prediction of a trough in the surface elevation at gauge 1 is about 6 cm (Figure 3), which is more than 50% of the measured trough depth. The greatest under-prediction at the crest is about 0.8 cm, which is about 6% of the measured crest height. Similarly for location 2 in Figure 4, we see an over-prediction of the trough of 4 cm and an under-prediction of the crest of 2.3 cm, which correspond to 34% and 15% of the measured trough depth and crest height, respectively.

The measured and predicted energy spectra at gauges 1 and 2 are presented in Figures 5 and 6. At the spectral peak, the surface elevation estimates based on both linear and nonlinear wave theory tend to overpredict the surface elevation spectrum estimated from the surface-piercing wave gauge; however, the nonlinear spectral estimates provide better agreement. At lower (0.07 to 0.20 Hz) and higher (1.0 to 2.0 Hz) frequencies, the predictions given by the nonlinear wave model agree better with the observed surface measurements than the spectra estimated using linear wave theory. The latter tends to overpredict the energies at high frequencies that are coincident with the sum-frequency range of the components near the spectral peak.

The under-/over- predictions by linear wave theory are a result of neglecting the combined effects of wave-wave interaction in the irregular wave field and the effects of short waves riding along longer waves. A qualitative explanation for the discrepancies between linear wave theory and the nonlinear model is given below.

In a transient or irregular wave train, wave components with different frequencies may interact. Large crests and troughs can be produced when wave components of different frequencies constructively interfere. Short (or high-frequency) waves superposed on a surface of long (or low-frequency) waves behave differently than short waves traveling on a calm sea. The wavelength of the short waves decreases at the crests of the long waves and increases in the troughs (LONGUET-HIGGINS and STEWART, 1960). Further, the distance between the short-wave components and the pressure transducer becomes greater or smaller relative to the mean water level, depending upon whether the short wave is at a crest or trough of the long wave. It is well known that wave-induced dynamic pressure decays exponentially with increased depth. Thus, the measured dynamic pressure at a fixed depth induced by the short-wave components will be greater under the long-wave trough than under its crest.

Linear wave theory ignores this interaction among wave components by evaluating the surface elevation from the dynamic pressure of each individual wave component relative to the mean water depth. Therefore, linear wave theory interprets larger dynamic pressure under troughs as larger trough heights and smaller dynamic pressure under crests as

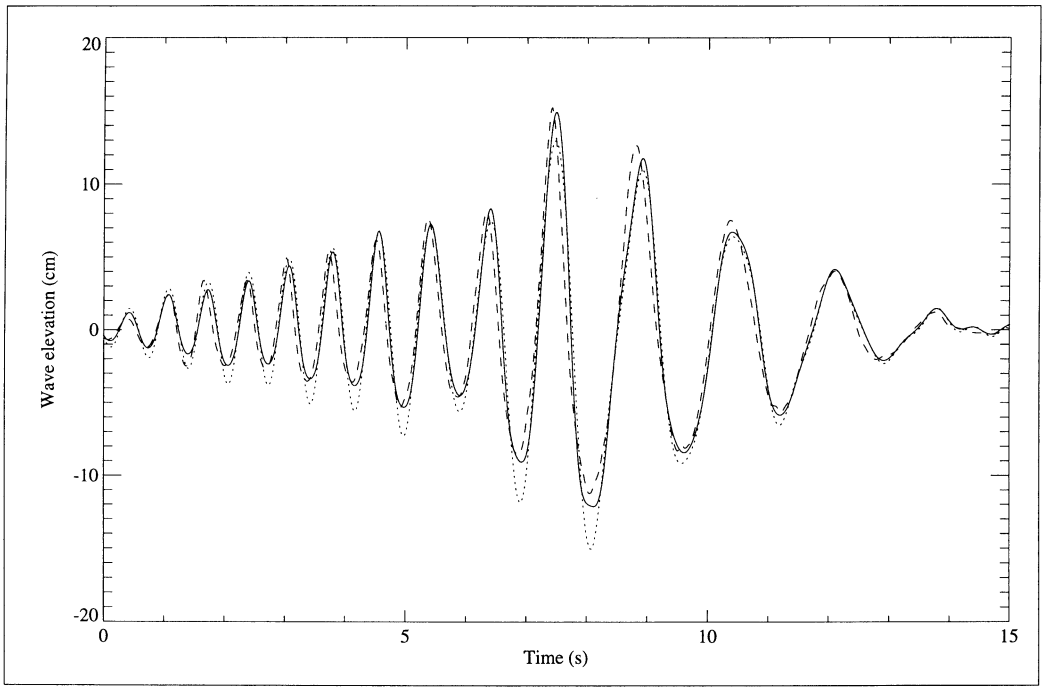

Figure 4. Observed (dashed) and predicted wave elevation at gauge 2 using linear (dotted) and nonlinear (solid) theory.

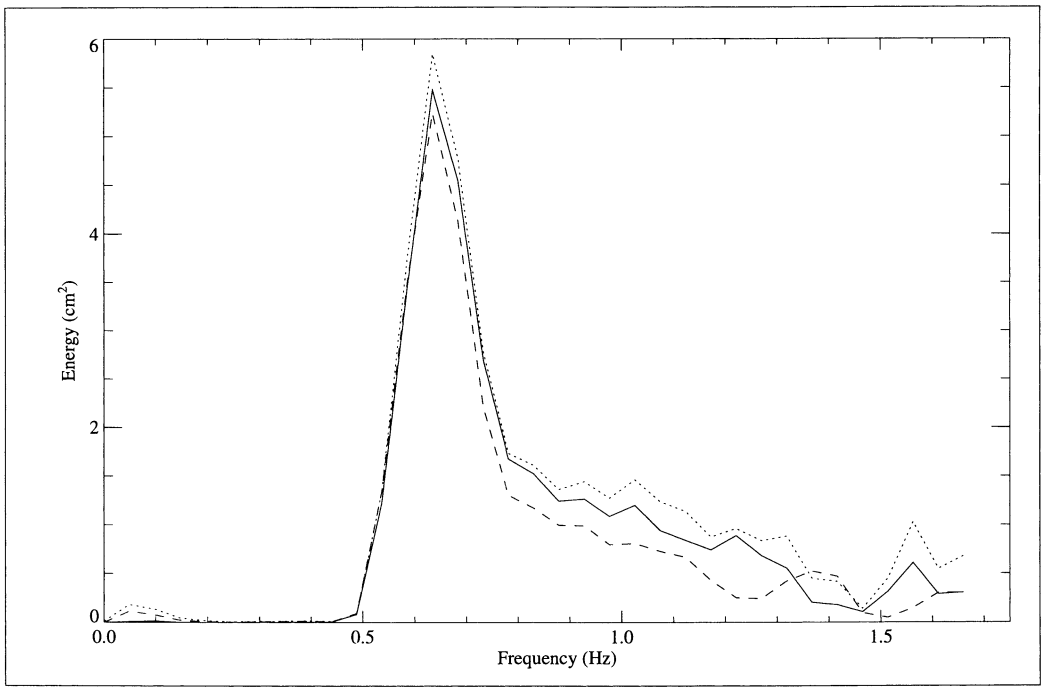

Figure 5. Observed (dashed) and predicted wave elevation spectra at gauge 1 using linear (dotted) and nonlinear (solid) theory.

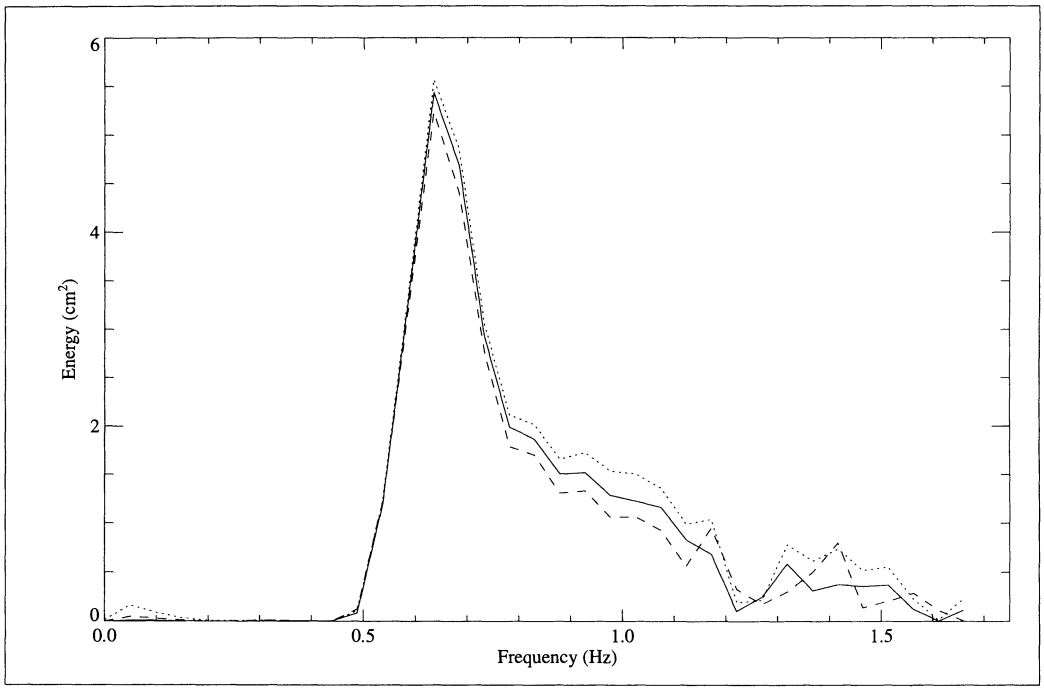

Figure 6. Observed (dashed) and predicted wave elevation spectra at gauge 2 using linear (dotted) and nonlinear (solid) theory.

smaller crest heights. The corresponding over- and underpredictions can be significant for waves with large wave heights where the crest and trough heights of long-wave components are relatively large. Such conditions existed south of Louisiana during Hurricane Andrew.

DESCRIPTION OF HURRICANE DATA

The instrument deployed south of Terrebonne Bay was a Coastal Leasing, Inc., MiniSpec directional wave gauge. The gauge was housed in a metal frame and measured dynamic pressure with an ICS solid state pressure transducer (0.84 hPa = 0.012 psia resolution) and horizontal current velocity with a Marsh-McBirney two-axis electromagnetic current meter. The pressure transducer was approximately 1 m off bottom and the current meter was approximately 1.3 m off bottom. The mean water depth at this location was approximately 20 m. The instrument was configured to measure 2048 pressure and current velocity samples at 2 Hz every two hours. The 2048 samples constituted a burst that lasted roughly 17 minutes. At the time the hurricane made its closest approach, between 2100 UTC and 2300 UTC 25 August 1992, the bottom-mounted frame and instrument were turned onto their sides due to strong bottom currents in excess of 1 m s^{-1}. Because the current sensor was no longer horizontal, the velocity data recorded after this time were discarded. The pressure sensor, however, continued to record at 0.2 m above bottom throughout the duration of the hurricane.

Because wave current velocity information was lost when the instrument was turned onto its side, we assume the wave field to be unidimensional, *i.e.,* all components traveling in the same direction. This is consistent with HERBERS and GUZA (1994) who showed that in strong and steady winds, colinear interactions are expected to dominate the pressure field below about 0.3 Hz. Assuming a one-dimensional wave field, we decomposed the measured wave field of 24 wave bursts recorded during the hurricane into a series of free-wave components using the nonlinear wave model described in Section 2. The free-wave components were truncated at 0.20 Hz. The sea surface was then estimated using the prediction scheme described in Section 2. Significant wave height, H_{mo}, was estimated from the linear sea surface spectrum of the 2048 samples of each burst and from the total variance of the nonlinear sea surface time series.

All spectra in the following section were constructed by averaging the spectral energy density of eight subsamples of each 2048-point wave elevation time series. Each subsample is 256 points and a Hanning filter was applied in the time domain to reduce spectral leakage. This procedure yields 16 degrees of freedom for each spectral component.

WAVE ELEVATION DURING HURRICANE ANDREW

Hurricane Andrew was a compact but intense hurricane that crossed the southern tip of Florida and entered the eastern Gulf of Mexico on 24 August 1992. STONE and FINKL (1995) review the key meteorological and hydrological aspects of this storm. DIMARCO *et al.* (1995) present the directional wave environment along the Texas-Louisiana shelf as measured by four bottom-mounted wave gauges. As the storm crossed the eastern limb of the Texas-Louisiana shelf, it at-

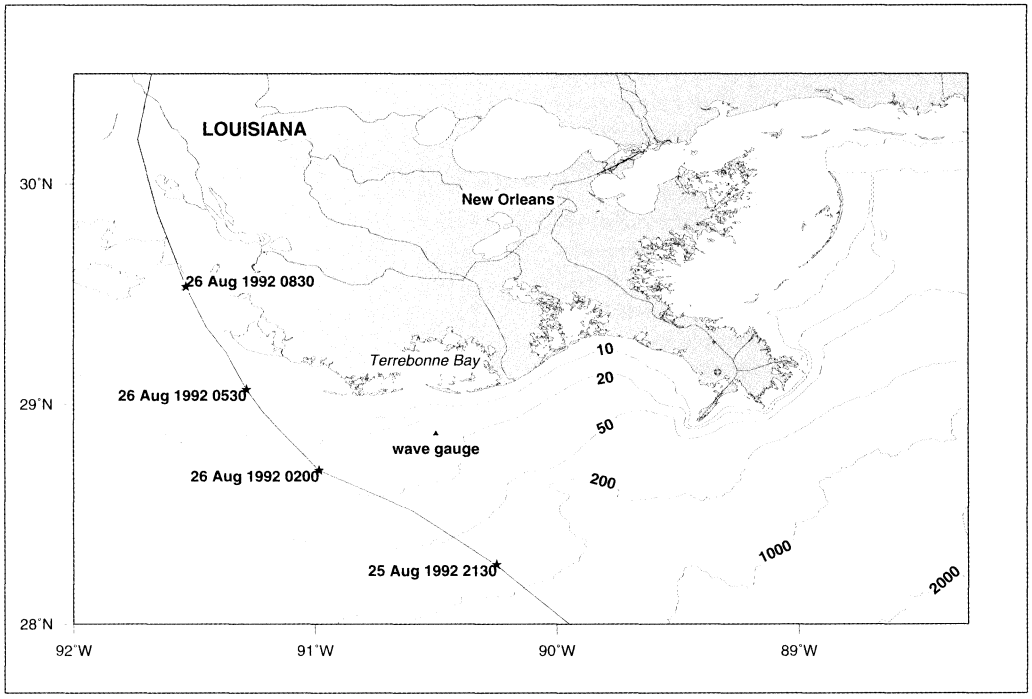

Figure 7. Map of the eastern Texas-Louisiana shelf region showing local bathymetry (m), wave gauge location, and Hurricane Andrew storm track. All times are UTC.

tained Category 4 status (SIMPSON and RIEHL, 1981) with sustained wind speeds of 63 m s^{-1}. The eye passed within 30 km of a near-bottom mounted wave gauge located 20 km south of Terrebonne Bay, Louisiana, 28.8671°N, 90.4908°W (Figure 7). Observational wave data on a continental shelf during extreme storm events are rare and the proximity of this site to the storm center make it of particular importance. Maximum wind speeds associated with the storm as it approached this location at 2100 UTC 25 August 1992 were 74 m s^{-1} (63 m s^{-1} sustained) (STONE *et al.,* 1993). The peak significant wave height at this site, estimated using linear wave theory and a high-frequency cutoff of 0.222 Hz, was 9.09 m and occurred at 0100 UTC 26 August 1992 with a peak spectral period between 10 and 12 s (DIMARCO *et al.,* 1995). The full linear wave spectrum at this time, however, contained a secondary peak around 6 s. The secondary spectral peak was initially believed to be the combined result of local wind forcing and nonlinear sum-frequency wave generation of interacting spectral components of the primary peak. The primary peak was thought to be mostly swell generated by the storm as it crossed the deep part of the eastern Gulf. The wave spectrum estimated at 2300 UTC 25 August 1992 was previously identified (DIMARCO *et al.,* 1995) to be a candidate where particularly strong nonlinear interaction may have occurred. We now focus on this spectrum to quantify its nonlinear properties and estimate the significant wave height using the nonlinear theory described in Section 2.

Figure 8 shows the spectral energy density estimated at the pressure sensor and at the surface using linear wave theory. The pressure transducer was about 19.5 m below the mean sea surface; therefore, the free-wave components at relatively high wave frequencies were expected to be greatly attenuated near bottom. The pressure amplitudes of periods between 5 and 7 seconds were small compared with the amplitude at the spectral peak, but are significantly greater than those of the background noise floor. The peak pressure spectral component occurs at 0.0859 Hz (period = 11.6 s).

After correlating the pressure spectrum for hydrodynamic attenuation using linear theory, the surface spectrum is seen to be doubly peaked, with the primary spectral peak occurring at 0.0859 Hz (period = 11.6 s) and a secondary peak in the range between 0.14 and 0.19 Hz (period 5 to 7 s). The secondary energy peak is at approximately twice the fundamental frequency, 0.1719 Hz (period 5.8 s). The significant wave height estimated from the sea surface spectrum shown in Figure 8 is 8.43 m.

Because the surface waves during the peak of the hurricane were steep, we surmise that the pressure energy near the period of 5 – 7 s in Figure 8 was partially the result of sum-frequency interactions of the wave components near the principal spectral peak. Figure 9 shows the predicted surface spectral energy density based on nonlinear and linear theory. The energy in the high-frequency band is substantially reduced, while the energy in the low-frequency band remains unchanged.

Portions of the predicted wave elevations as a function of time using the nonlinear and linear wave theory are plotted in Figure 10. We see that the predicted trough depths using linear wave theory are consistently deeper than those estimated using the nonlinear wave model, especially for deep

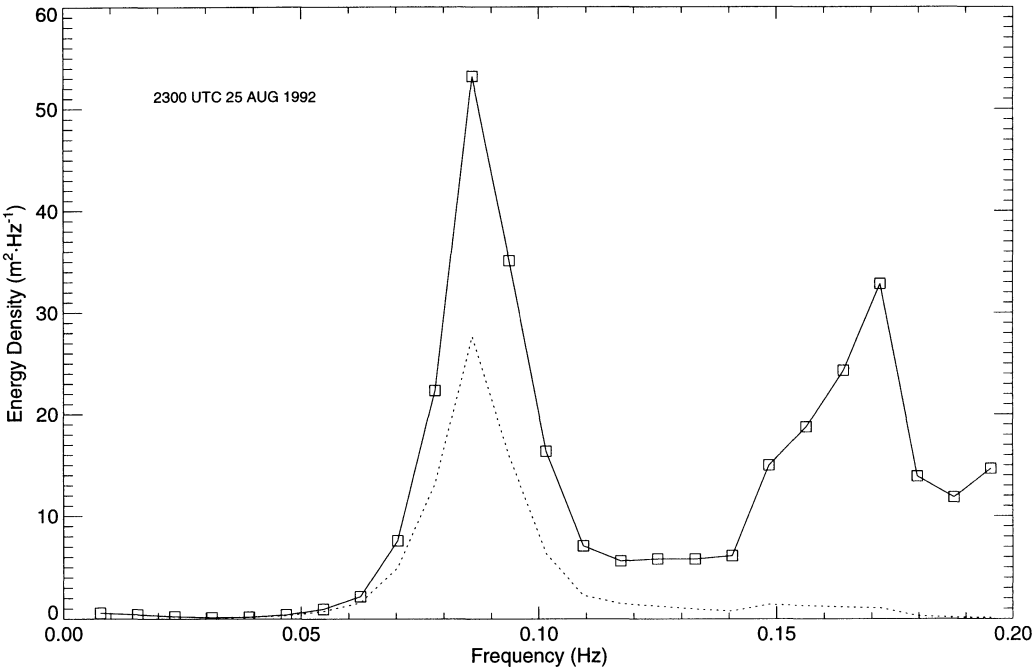

Figure 8. Energy density spectrum of surface (solid) and bottom pressure (dashed) time series recorded south of Terrebonne Bay, Louisiana, at 2300 UTC 25 August 1992. Spectral estimates have 16 degrees of freedom. Sea surface estimated using linear wave theory.

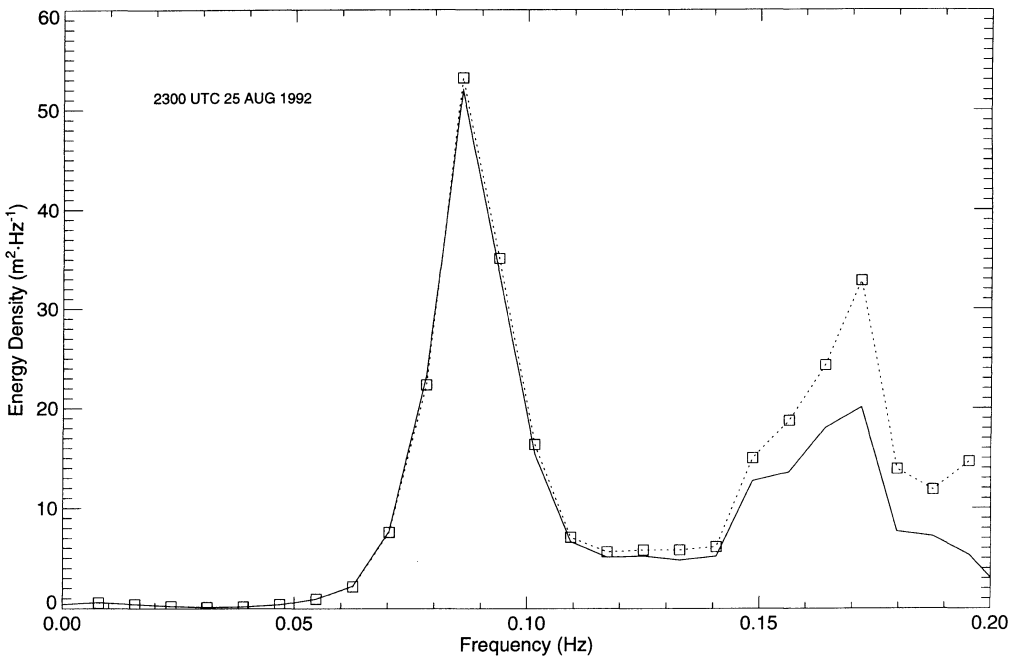

Figure 9. Energy density spectrum of sea surface elevation estimated using linear (dashed) and nonlinear (solid) theory at 2300 UTC 25 AUG 1992. Spectral estimates have 16 degrees of freedom.

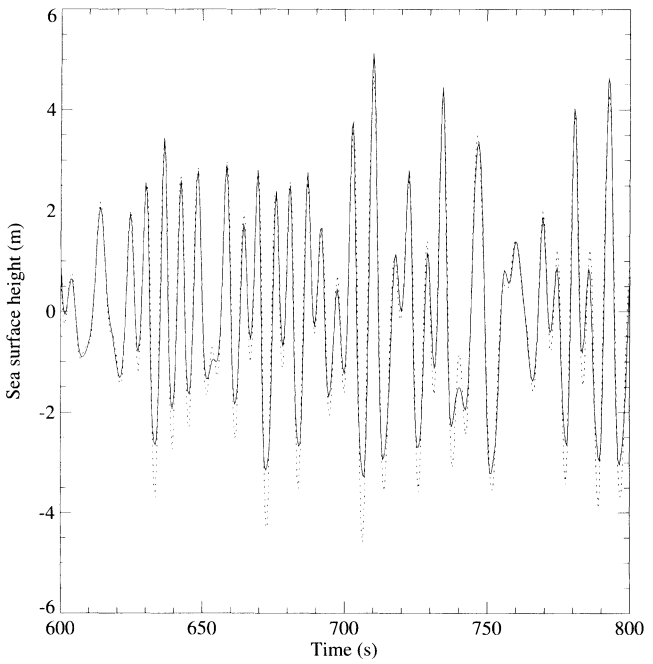

Figure 10. Sea surface time series estimated from linear (dashed) and nonlinear wave model (solid) spectra using pressure time series recorded at 2300 UTC 25 August 1992. Time is in seconds from beginning of burst.

troughs. For the eleven wave troughs in Figure 10 that are less than −3 m (based on linear theory), the estimated troughs are an average of 24% shallower than the troughs estimated using nonlinear theory. However, for the seven wave crests in Figure 10 that are greater than 4 m (estimated from linear theory), the crests are on average 3% smaller than the nonlinear wave crests.

The differences in the predicted crest and trough heights by linear and nonlinear wave theory are consistent with those observed in the case of the transient wave train produced in the wave flume (Section 3). The smaller differences in the crest heights compared to the differences in trough depth for the case of Hurricane Andrew is also consistent with the laboratory results. However, further testing has shown that a pressure transducer closer to the surface yielded trough and crest differences of the same order.

As expected, linear wave theory over-predicts the amplitudes of frequencies which match the sum-frequencies resulting from the interactions among wave components near the major peak. The predicted spectrum from nonlinear theory has energy beyond the cut-off frequency of 0.20 Hz that results from the sum-frequency interactions among the free-wave components of frequencies below the cut-off frequency.

Figure 11 shows the linear and nonlinear estimated significant wave height time series for the 24 hours prior to and following the hurricane's closest approach to the wave gauge. The significant wave heights prior to Andrew are less than 1.5 m with peak spectral periods of 5–6 seconds. As the long period swell arrives the wave height increases and the peak spectral periods increase to 10–12 seconds. During the time

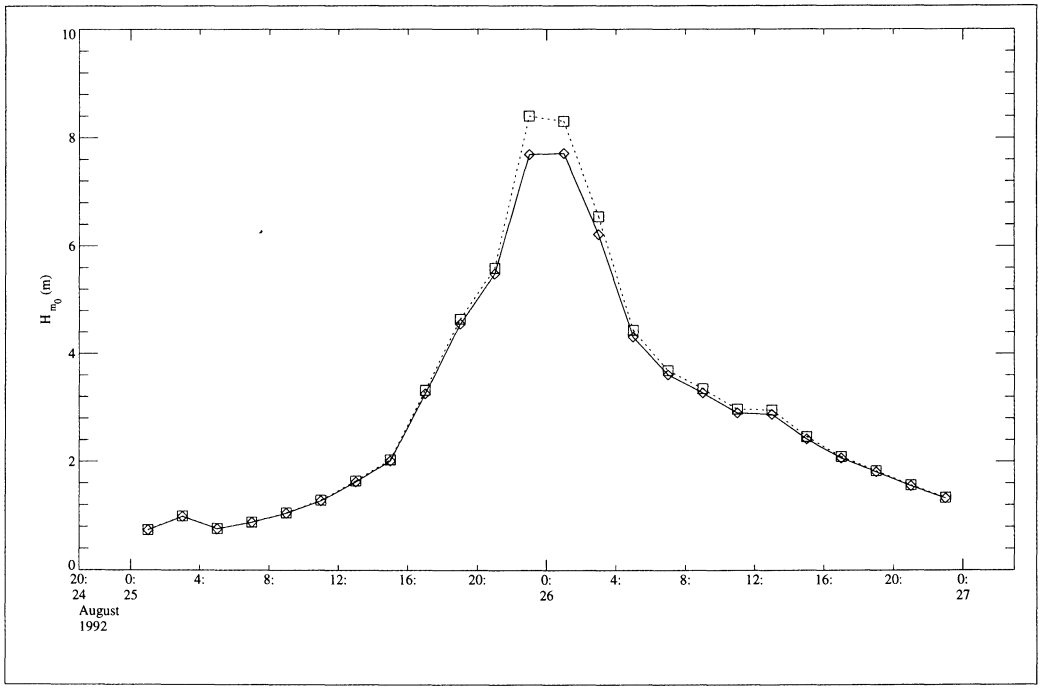

Figure 11. Significant wave height, H_{mo}, estimated using linear (dashed) and nonlinear (solid) wave theory from near-bottom pressure data recorded south of Terrebonne Bay, Louisiana, during Hurricane Andrew. Times are UTC.

Table 1. *Significant wave height (m) during Hurricane Andrew south of Terrebonne Bay, LA, based on linear (L) and nonlinear theory (NL) (0.20 Hz cutoff)*

Date	Time (UTC)	$H_{m_0}^{L}$	$H_{m_0}^{NL}$	% change
08/25	01:00	0.74	0.74	0.53
08/25	03:00	1.00	0.99	0.94
08/25	05:00	0.77	0.76	0.50
08/25	07:00	0.89	0.88	0.58
08/25	09:00	1.06	1.05	0.82
08/25	11:00	1.29	1.28	1.00
08/25	13:00	1.65	1.63	1.22
08/25	15:00	2.04	2.02	1.02
08/25	17:00	3.33	3.26	1.96
08/25	19:00	4.65	4.56	1.98
08/25	21:00	5.60	5.49	1.93
08/25	23:00	8.40	7.69	8.43
08/26	01:00	8.31	7.71	7.12
08/26	03:00	6.55	6.22	5.02
08/26	05:00	4.44	4.31	2.85
08/26	07:00	3.69	3.61	2.17
08/26	09:00	3.35	3.28	2.29
08/26	11:00	2.98	2.91	2.33
08/26	13:00	2.96	2.88	2.68
08/26	15:00	2.46	2.42	1.82
08/26	17:00	2.09	2.07	1.24
08/26	19:00	1.83	1.81	1.10
08/26	21:00	1.57	1.55	0.96
08/26	23:00	1.34	1.32	0.97

period 2100 UTC 25 August to 0400 UTC 26 August 1992, the ocean currents and waves were driven by hurricane force winds. It is during this period that the linear energy spectra had strong spectral peaks with periods in excess of 10 s, and the nonlinear effects were the largest. The largest significant wave height during Andrew was estimated at 0100 UTC 26 August 1992. After the storm made landfall and continued inland (0830 UTC 26 August), the significant wave height and peak spectral period gradually decreased.

The effects of the nonlinear interaction change the significant wave height from 0–2% before and after the storm. During the approximately six-hour period of the storm's passage over the gauge, the significant wave height is reduced from 5-8% when using the nonlinear model. After the storm, the low-frequency swell continued to pass for several hours, which is important to the estimation of relatively high-frequency wave elevations. As a result, we see a 2–3% difference between the estimated significant wave heights by linear and nonlinear methods. As the wave height decreases and the peak spectral frequency increases, the nonlinear interaction begins to weaken. Table 1 summarizes the linear and nonlinear significant wave height estimates during Hurricane Andrew.

An analysis of current meter records in a line across the Texas-Louisiana shelf along 90° W shows that after the hurricane made landfall the response of the waters on the shelf was to oscillate inertially, *i.e.,* in an anticyclonic (clockwise) manner and with local inertial period. The surface velocity record at the wave gauge location was lost, but it can be inferred from other nearby velocity records that the currents at the wave gauge were strong and northeasterly. The surface wave propagation direction was probably westerly, although the precise direction is not known. The slight increase in wave height at around 1300 UTC 26 August 1992 may be related to a wave-current interaction as the waves propagated in the opposite direction from the prevailing current. However, a direct estimation of the wave-current interaction is not possible because of the lack of current velocity data at this location.

Figure 12 shows contours of the spectral energy density based on nonlinear (right) and linear (left) theory as a function of time centered at the time of the storm's closest approach. We see that the energy associated with low frequency waves is unchanged when considering the nonlinear interaction, but energy associated with high-frequency waves is substantially reduced, particularly when the storm passes closest to this location.

As was seen above, the sea surface trough depths were over-predicted by linear theory. Therefore, the mean water depth during the burst estimated using linear theory will be slightly different than that estimated from the nonlinear wave model. Figure 13 shows the mean water depth for each burst during the passage of the hurricane as estimated from the nonlinear wave model. The storm surge range is approximately 1.5 m with the largest rate of change occurring simultaneously with the largest nonlinear interaction beginning 2100 UTC 25 August 1992. The peak surge occurs at 0500 UTC 26 August 1992, when the eye was approximately 60 km west of the site. The water level gradually recedes to pre-storm levels 15–20 hours after the peak high water. Because the mean water level changed by only a small amount, the nonlinear result should only be regarded as a perturbation. The change in mean water height is consistent with storm surge measurements of 1.0 to 1.5 m taken during Hurricane Andrew at tide stations in the vicinity of Terrebonne Bay, Louisiana (BREAKER *et al.,* 1994).

CONCLUSIONS

We have shown that nonlinear wave theory more accurately predicts the surface elevation from a pressure time series than does linear wave theory. Laboratory flume tests confirm that the nonlinear theory more accurately predicts the sea surface elevation of an irregular wave train especially for deep troughs and high crests. We applied the nonlinear model to a unique near-bottom dynamic pressure data set recorded within 30 km of the eye of Hurricane Andrew. The significant wave height estimated at this site was reduced by as much as 8.4% when using the nonlinear model. The largest differences in significant wave heights occurred when the storm was directly overhead. An analysis of the average sea surface elevation shows that storm surge associated with Hurricane Andrew was approximately 1.5 m and in agreement with tide stations in the vicinity of Terrebonne Bay, Louisiana.

ACKNOWLEDGEMENTS

This study was supported in part by the Offshore Technology Research Center of the National Science Foundation under Contract CDR-8721512 (J.Z. and E.M.C) and by the U.S. Minerals Management Service under OCS Contract 14-35-0001-30509 (S.F.D.). Additional funding has been provided by Texas A&M University, the Texas Engineering Experiment Station, and the Texas Institute of Oceanography (S.F.D.).

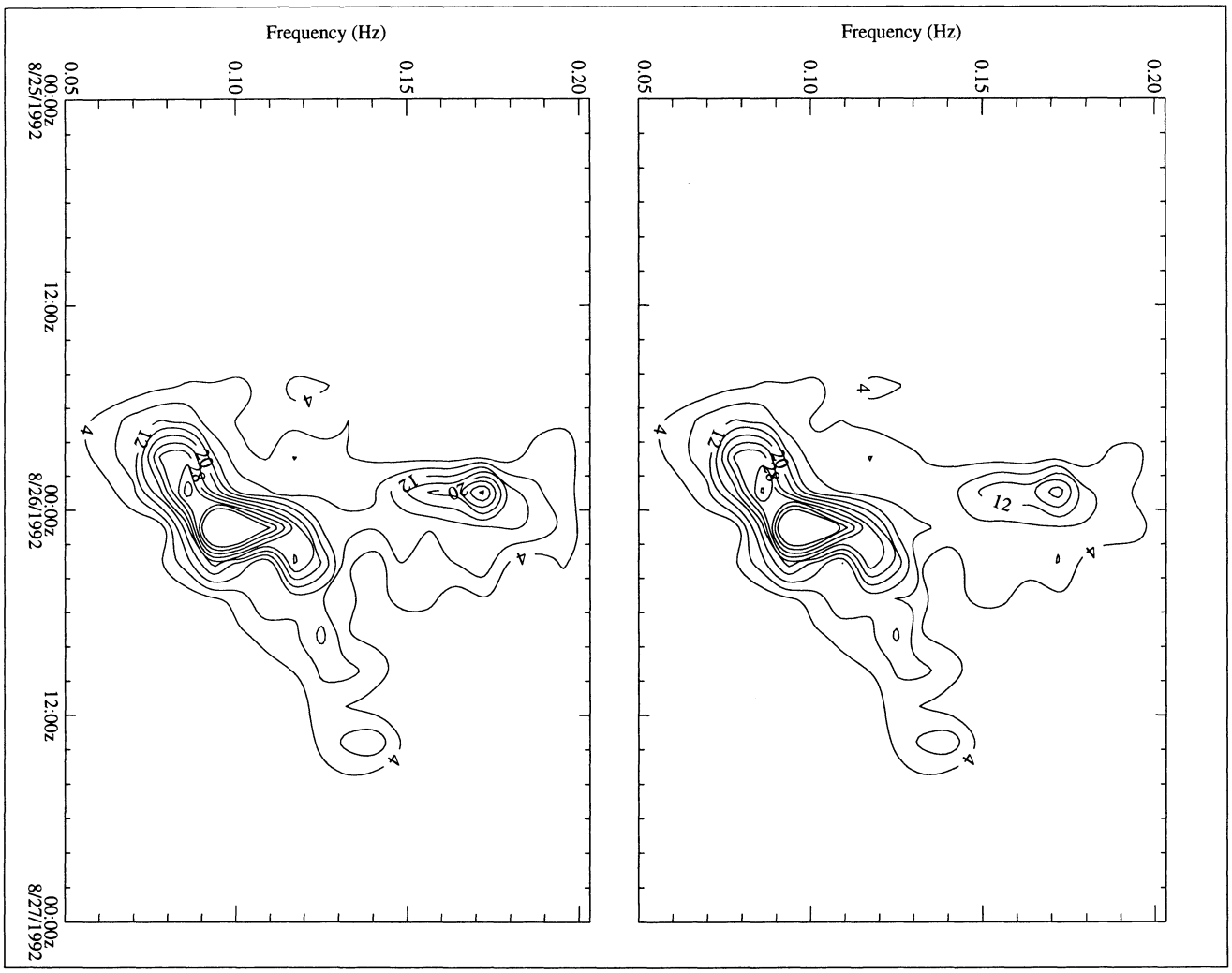

Figure 12. Contour plot of spectral energy density (m^2 Hz^{-1}) south of Terrebonne Bay, Louisiana, during Hurricane Andrew using nonlinear (right) and linear theory (left). Contour interval is 4 m^2 Hz^{-1}.

The authors would like to thank L. C. Bender and R. O. Reid for useful discussions relating to this work. Special thanks go to J. Heideman for useful discussions and for providing the motivation for pursuing this research.

APPENDIX
COEFFICIENTS IN NONLINEAR POTENTIAL, ELEVATION, AND DISPERSION RELATION

The following coefficients are the nonlinear sum- and difference-frequency amplitudes shown in Eq. 3.

$$A_{j+i} = \frac{a_i a_j \sigma_j (1 + \alpha_i \alpha_j)}{2} \times \left[\frac{-(1 - \alpha_i{}^2)\lambda_{i,j}{}^3 - 2(1 - \alpha_i \alpha_j)(\lambda_{i,j}{}^2 + \lambda_{i,j}) + \alpha_j{}^2 - 1}{(\lambda_{i,j}\alpha_i - \alpha_j)^2 - (\lambda_{i,j} + 1)^2} \right],$$

$$A_{j-i} = \frac{a_i a_j \sigma_j (1 - \alpha_i \alpha_j)}{2} \times \left[\frac{(1 - \alpha_i{}^2)\lambda_{i,j}{}^3 - 2(1 + \alpha_i \alpha_j)(\lambda_{i,j}{}^2 - \lambda_{i,j}) + \alpha_j{}^2 - 1}{(\lambda_{i,j}\alpha_i - \alpha_j)^2 - (\lambda_{i,j} - 1)^2} \right], \quad (8)$$

where $\alpha_i = \coth(k_i h)$, ($i = 1$ or 2) and $\lambda_{i,j} = \sigma_i/\sigma_j$ where $i < j$ and $\sigma_i < \sigma_j$.

The nonlinear hydrodynamic attenuation coefficients in Eq. 5 are:

$$K_{i,j}{}^{C\pm} = \frac{\cosh((k_j \pm k_i)(z + h))}{\cosh((k_j \pm k_i)h)},$$

$$K_{i,j}{}^{S\pm} = \frac{\cosh((k_j \pm k_i)(z + h))}{\sinh(k_i h)\sinh(k_j h)}. \quad (9)$$

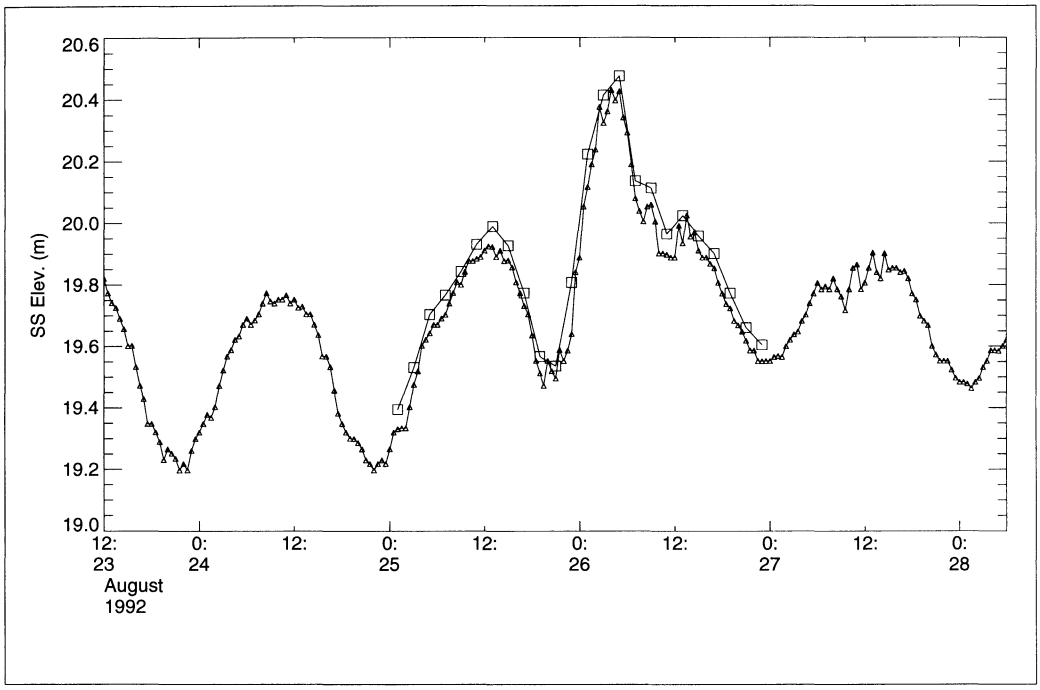

Figure 13. Average sea surface height above bottom estimated using nonlinear theory (squares) and average pressure converted to meters of water (triangles) showing storm surge south of Terrebonne Bay, Louisiana, during Hurricane Andrew.

The following coefficients are used in the calculation of the nonlinear dispersion relation shown in Eq. 7.

$$S_i = k_i^2\left[\frac{9}{8}(\alpha_i^2 - 1)^2 + \alpha_i^2\right], \tag{10}$$

$$\begin{aligned} Q_{ij} = {} & -\frac{1}{2\alpha_j^2}[(\alpha_j\beta_s - 1)SX_{ij} - (\alpha_j\beta_r - 1)RX_{ij}]\frac{\sigma_j}{\sigma_i}k_j^2 \\ & + \frac{1}{2\alpha_j^2}(\alpha_j + 1)[1 + SX_{ij} + RX_{ij}]k_j^2 \\ & + \frac{\alpha_i}{\alpha_j}\left[(1 + SX_{ij} + RX_{ij}) - \frac{\beta_s}{2}\left(\frac{1}{\alpha_i} + \frac{1}{\alpha_j}\right)SX_{ij}\right. \\ & \left. + \frac{\beta_r}{2}\left(\frac{1}{\alpha_i} - \frac{1}{\alpha_j}\right)RX_{ij}\right]\frac{\sigma_i}{\sigma_j}k_j^2 \\ & - \frac{1}{2}\left[\left(\frac{\alpha_i}{\alpha_j}\right)(\alpha_i^2 + 1) + 2(RX_{ij} - SX_{ij})\right]k_ik_j \\ & + \frac{1}{2\alpha_j}[(\alpha_i - 1)SX_{ij} - (\alpha_i + 1)RX_{ij} + 2\alpha_j]\frac{\sigma_i}{\sigma_j}k_ik_j, \end{aligned} \tag{11}$$

and

$$RX_{12} = \frac{A_{j-i}}{a_ia_j\sigma_j}, \qquad SX_{12} = \frac{A_{j+i}}{a_ia_j\sigma_j}, \tag{12}$$

$$\beta_r = \frac{\alpha_j - \alpha_i}{1 - \alpha_i\alpha_j}, \qquad \beta_s = \frac{\alpha_j + \alpha_i}{1 + \alpha_i\alpha_j}. \tag{13}$$

We note that the deep water solutions for the nonlinear potential, elevation, and dynamic pressure can readily be obtained by allowing $h \to \infty$ and $\alpha_i \to 1$ and $\alpha_j \to 1$.

LITERATURE CITED

BREAKER, L. C.; BURROUGHS, L. D.; CHAO, Y. Y.; CULP, J. F.; GUINASSO, N. L., JR; TEBOULLE, R. L., and WONG, C. R., 1994. The Impact of Hurricane Andrew on the Near Surface Marine Environment in the Bahamas and the Gulf of Mexico. *Weather and Forecasting,* 9(4), 542–556.

DIMARCO, S. F.; KELLY, F. J.; ZHANG, J., and GUINASSO, N. L. JR., 1995. Directional Wave Spectra on the Louisiana-Texas Shelf During Hurricane Andrew. *J. Coastal Res.,* Spring, Vol. SI-21, p. 217–233.

HASSELMANN, K., 1962. On the nonlinear energy transfer in a gravity-wave spectrum. Part 1: General theory. *J. Fluid Mech.,* 12, 481–500.

HERBERS, T. H. C. and GUZA, R. T., 1991. Wind-wave nonlinearity observed on the sea floor. Part I: Forced-wave energy. *J. Phys. Ocn.,* 21(12), 1740–1761.

HERBERS, T. H. C. and GUZA, R. T., 1992. Wind-wave nonlinearity observed on the sea floor. Part II: Wavenumbers and third-order statistics. *J. Phys. Ocn.,* 22(5), 489–504.

HERBERS, T. H. C. and GUZA, R. T., 1994. Non-linear wave interactions and high-frequency sea floor pressure. *J. Geo. Res.,* 99(5), 10035–10048.

LONGUET-HIGGINS, M. S. and STEWART, R. W., 1960. Changes in the form of short gravity waves on long waves and tidal currents. *J. Fluid Mech.,* 8, 565–583.

PHILLIPS, O. M., 1960. On the dynamics of unsteady gravity waves of finite amplitude. Part 1: The elementary interactions. *J. Fluid Mech.,* 9, 193–217.

PRISLIN, I.; ZHANG, J., and SEYMOUR, R. J., 1997. Deterministic Decomposition of Short Crested Irregular Gravity Waves. *J. Geo. Res.,* 102(C6), 12677–12688.

RODENBUSCH, G. and FORRISTALL, G. Z., 1986. An empirical model

for random directional wave kinematics near the free surface. *Proc. 18th Annual Offshore Technology Conference,* OTC **5097,** Houston, Texas.

SIMPSON, R. H. and RIEHL, H., 1981. *The Hurricane and Its Impact.* Baton Rouge, Louisiana: LSU Press. 398 pp.

SPELL, C. A.; ZHANG, J., and RANDALL, R. E., 1996. Hybrid wave model for unidirectional irregular waves, Part II. Comparison with Laboratory Measurements. *J. Appl. Ocn. Res.,* **18,** 93–110.

STONE, G. W.; GRYMES, J. M., III; ROBBINS, K. D.; UNDERWOOD, S. G.; STEYER, G. D., and MULLER, R. A., 1993. A Chronologic Overview of Climatological and Hydrological Aspects Associated with Hurricane Andrew and its Morphological Effects Along Louisiana Coast, U.S.A. *Shore and Beach,* 61(2), 2–12.

STONE, G. W. and FINKL, C. W., 1995. A Review of the Key Meteorological and Hydrological Aspects of Hurricane Andrew. *J. Coastal Res.,* Spring, Vol. SI-21, p. 1–5.

YUEN, H. C. and LAKE, B. M., 1982. Nonlinear dynamics of deep-water gravity waves. *Adv. Appl. Mech.,* 22, 67–229.

ZHANG, J.; CHEN, L.; YE, M., and RANDALL, R. E., 1996. Hybrid Wave model for unidirectional irregular waves, Part I. Theory and Numerical Scheme. *J. Appl. Ocn. Res.,* **18,** 77–92.

ZHANG, J.; HONG, K., and YUE, D. K. P., 1993. Effects of wavelength ratio on wave modeling. *J. Fluid Mech.,* Vol. 248, pp. 107–127.

ZHANG, J.; MEZA CONDE, E., and SEYMOUR, R. J., 1997. Experimental Studies on energy dissipation in breaking waves. *Proceedings of 7th ISOPE Conference,* May 25–30, Honolulu, HI.

ZHANG, J.; PRISLIN, I.; YANG, J., and WEN, J., 1999b. Deterministic wave model for short-crested ocean waves: Part II. Comparison with laboratory and field measurements. *Appl. Ocn. Res.,* 21, 189–206.

ZHANG, J., RANDALL, R. E., and SPELL, C. A., 1991. On wave kinematics approximate methods. *Proceedings of 23rd Offshore Technology Conference,* OTC **6522,** Houston, Texas. pp. 231–238.

ZHANG, J.; YANG, J.; WEN, J.; PRISLIN, I., and HONG, K., 1990a. Deterministic wave model for short-crested ocean waves: Part I. Theory and numerical scheme. *Appl. Ocn. Res.,* 21, 167–188.